Thermally Activated Site Exchange and Quantum Exchange Coupling Processes in Unsymmetrical Trihydride Osmium Compounds

Amaya Castillo,[†] Guada Barea,[‡] Miguel A. Esteruelas,*[,†] Fernando J. Lahoz,[†] Agustí LLedós,*[,‡] Feliu Maseras,[‡] Javier Modrego,[†] Enrique Oñate,[†] Luis A. Oro,[†] Natividad Ruiz,[†] and Eduardo Sola[†]

Departamento de Química Inorgánica, Instituto de Ciencia de Materiales de Aragón, Universidad de Zaragoza−CSIC, 50009 Zaragoza, Spain, and Unitat de Química Física, Departament de Química, Universitat Autònoma de Barcelona, 08193 Bellaterra, Barcelona, Spain

Received April 9, 1998

Reaction of the hexahydride complex $OsH_6(P^iPr_3)_2$ (**1**) with pyridine-2-thiol leads to the trihydride derivative $OsH_3\{\kappa\text{-}N,\kappa\text{-}S\text{-}(2\text{-Spy})\}(P^iPr_3)_2$ (**2**). The structure of **2** has been determined by X-ray diffraction. The geometry around the osmium atom can be described as a distorted pentagonal bipyramid with the phosphine ligands occupying axial positions. The equatorial plane contains the pyridine-2-thiolato group, attached through a bite angle of 65.7(1)°, and the three hydride ligands. The theoretical structure determination of the model complex $OsH_3\{\kappa\text{-}N,\kappa\text{-}S\text{-}(2\text{-Spy})\}(PH_3)_2$ (**2a**) reveals that the hydride ligands form a triangle with sides of 1.623, 1.714, and 2.873 Å, respectively. A topological analysis of the electron density of **2a** indicates that there is no significant electron density connecting the hydrogen atoms of the OsH_3 unit. In solution, the hydride ligands of **2** undergo two different thermally activated site exchange processes, which involve the central hydride with each hydride ligand situated close to the donor atoms of the chelate group. The activation barriers of both processes are similar. Theoretical calculations suggest that the transition states have a *cis*-hydride−dihydrogen nature. In addition to the thermally activated exchange processes, complex **2** shows quantum exchange coupling between the central hydride and the one situated close to the sulfur atom of the pyridine-2-thiolato group. The reactions of **1** with L-valine and 2-hydroxypyridine afford $OsH_3\{\kappa\text{-}N,\kappa\text{-}O\text{-}OC(O)CH[CH(CH_3)_2]NH_2\}(P^iPr_3)_2$ (**3**) and $OsH_3\{\kappa\text{-}N,\kappa\text{-}O\text{-}(2\text{-Opy})\}(P^iPr_3)_2$ (**4**) respectively, which according to their spectroscopic data have a similar structure to that of **2**. In solution, the hydride ligands of **3** and **4** also undergo two different thermally activated site exchange processes. However, they do not show quantum exchange coupling. The tetranuclear complexes $[(P^iPr_3)_2H_3Os(\mu\text{-biim})M(TFB)]_2$ [M = Rh (**5**), Ir (**6**); H_2biim = 2, 2′-biimidazole; TFB = tetrafluorobenzobarrelene] have been prepared by reaction of $OsH_3(Hbiim)(P^iPr_3)_2$ with the dimers $[M(\mu\text{-OMe})(TFB)]_2$ (M = Rh, Ir). In solution the hydride ligands of these complexes, which form two chemically equivalent unsymmetrical OsH_3 units, undergo two thermally activated site exchanges and show two different quantum exchange coupling processes.

Introduction

^{1}H NMR spectra of transition metal compounds with more than one hydride ligand have revealed two types of temperature dependent phenomena. The first is a thermally activated site exchange process of the hydride ligands,[1] which is proposed to take place via η^2-H_2 structures.[2] This proposal has been reinforced by a detailed study of the exchange process in the cation $[RhH_2(PP_3)]^+$ [$PP_3 = P(CH_2CH_2PPh_2)_3$].[3] The observation of a kinetic isotope effect for the intramolecular hydride exchange suggests that the M−H interactions change significantly between the ground and transition states. Theoretical studies on the hydride exchange processes in the trihydride species $[CpIrH_3L]^+$ (L = PH_3, CO),[4] $OsH_3(BH_4)(PH_3)_2$,[5] and $[CpMH_3]^{n+}$ (M = Mo, W, n = 1; M = Nb, Ta, n = 0)[6] have led to the same conclusion: the exchange takes place through an η^2-H_2 transition state, which is reached by a shortening of the H−H distance and a lengthening of the M−H distances. A detailed analysis of the charge in the electronic M−H interactions along the hydride exchange process is offered in our present study.

A second temperature-dependent process is quantum exchange coupling shown by several trihydrides of Nb,[7] Mo,[7b] Ru,[8] Os,[9] and Ir.[10] This phenomenon consists of a temperature varying hydrogen−hydrogen coupling which increases with decreasing electron density at the hydride sites.[11] The coupling J_{obs} is a combination of J_{mag} and J_{ex} given by eq 1, where J_{mag} is the portion of J_{obs} due to the Fermi contact interaction and J_{ex} is that due to the quantum exchange coupling. The sign of

* Corresponding authors.
† Universidad de Zaragoza.
‡ Universitat Autònoma de Barcelona.

(1) (a) Moorl, D.; Robinson, S. D. *Chem. Soc. Rev.* **1983**, *12*, 415. (b) Kubas, G. J. *Acc. Chem. Res.* **1988**, *21*, 129. (c) Jessop, P. G.; Morris, R. H. *Coord. Chem. Rev.* **1992**, *121*, 155. (d) Crabtree, R. H. *Angew. Chem., Int. Ed. Engl.* **1993**, *32*, 789. (e) Heinekey, D. M.; Oldham, W. J. *Chem. Rev.* **1993**, *93*, 913. (f) Gusev, D. G.; Berke, H. *Chem. Ber.* **1996**, *129*, 1143.
(2) Bakhmutov, V. I.; Bürgi, T.; Burger, P.; Ruppli, U.; Berke, H. *Organometallics* **1994**, *13*, 4203.
(3) Heinekey, D. M.; Roon, M. V. *J. Am. Chem. Soc.* **1996**, *118*, 12134.
(4) Jarid, A.; Moreno, M.; Lledós, A.; Lluch, J. M.; Bertrán, J. *J. Am. Chem. Soc.* **1995**, *117*, 1069.
(5) Demachy, I.; Esteruelas, M. A.; Jean, Y.; Lledós, A.; Maseras, F.; Oro, L. A.; Valero, C.; Volatron, F. *J. Am. Chem. Soc.* **1996**, *118*, 8388.
(6) Camanyes, S.; Maseras; F.; Moreno, M.; Lledós, A.; Lluch, J. M.; Bertrán, J. *J. Am. Chem. Soc.* **1996**, *118*, 4617.

10.1021/ic9804061 CCC: $18.00
Published on Web 03/26/1999

the temperature invariant J_{mag} is not predicted by eq 1 and may vary from compound to compound. However, J_{ex} is inherently negative and is a function of the temperature.

$$J_{obs} = J_{mag} - 2J_{ex} \quad (1)$$

Limbach, Chaudret, and co-workers[12] have proposed that the exchange coupling involves an equilibrium between a ground state hydride complex and a thermally accessible dihydrogen compound, in which rotational tunneling gives rise to the anomalous behavior detected by ^{1}H NMR spectroscopy. On the other hand, Heinekey and co-workers[10c,d,11c] believe that the principal cause of this phenomenon is a soft vibrational potential allowing substantial delocalization of the hydrides in the molecule.

To rationalize the phenomenon, several computational studies have also been carried out. The quantum exchange coupling in the trihydride complexes $[CpIrH_3L]^+$ has been studied by combining the construction of ab initio potential energy surfaces with a tunneling model using a basis set method. The results of this calculation suggest that these species exchange a pair of hydrogen atoms through a tunneling path involving a M(η^2-H_2) transition state.[4] Along this line, Eisenstein[13] and co-workers have calculated the exchange coupling in $OsH_3X(PH_3)_2$ (X = Cl, I) by determining the eigenstates resulting from the coupling between the internal rotation and vibration modes, which correspond to the pairwise hydrogen exchange. The structure at the barrier maximum may involve a η^2-H_2 ligand but does not require one. Common to the results from the two studies is the need for a low energy barrier, i.e., a path for the exchange process which has an energy not too far above that of the minimum.

As part of our work on the osmium polyhydride chemistry,[14] we have previously reported the synthesis of the compounds OsH_3(Hbiim)(P^iPr_3)$_2$, (P^iPr_3)$_2H_3Os$(μ-biim)M(COD) (biim = 2,2′-biimidazolato, M = Rh, Ir),[14c] and $[OsH_3$(diene)(P^iPr_3)$_2$]-BF_4 (diene = 2,5-norbornadiene, tetrafluorobenzobarrelene),[14d] which are the first trihydride derivatives containing nitrogen-donor ligands and diolefins, respectively, that show quantum exchange coupling between the hydrogen nuclei of the symmetrical OsH_3 unit.

Continuing with the work in this field, we now describe the synthesis of new trihydride osmium compounds showing quantum exchange coupling which, in contrast to those mentioned above, contain an asymmetrical OsH_3 unit. In addition, we report the X-ray structure and theoretical characterization of one of them as well as a detailed analysis of the change in the Os−H interactions during the thermally activated exchange process.

The analysis of the Os−H interactions is performed with the aid of the "atoms in molecules" (AIM) theory developed by Bader and co-workers.[15] This kind of analysis has been used to study the nature of bonding in classical and nonclassical dihydride complexes,[16] and has been recently applied to a series of L_nMH_2 systems spanning a large range of H−H distances.[17] The AIM scheme is based on the topological analysis of the electron density and its associated gradient and Laplacian and allows an unequivocal assignment of the bond structure of the molecule.

Results and Discussion

1. Synthesis and X-ray Structure of $OsH_3\{\kappa$-*N*,κ-*S*-(2-Spy)$\}(P^iPr_3)_2$. Treatment of $OsH_6(PiPr_3)_2$ (**1**) with pyridine-2-thiol in 1:1 molar ratio, in boiling toluene gives, after 2 h, a yellow solution from which the pyridine-2-thiolato complex $OsH_3\{\kappa$-*N*,κ-*S*-(2-Spy)$\}(P^iPr_3)_2$ (**2**) can be separated as a yellow microcrystalline solid in 89% yield. The formation of **2** can be rationalized in terms of the loss of four hydrogen atoms as molecular hydrogen, accompanied by the chelation of the pyridine-2-thiolato anion to the central metal (eq 2).

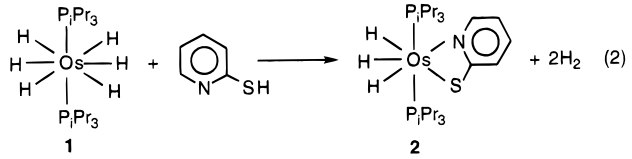

The first step of the reaction may be the protonation of **1** to give a cationic dihydrogen intermediate, probably $[OsH_3(\eta^2$-$H_2)_2(P^iPr_3)_2]^+$, which rapidly reacts with the pyridine-2-thiolato anion to afford **2**. In this context, it is worthwhile to note that a variety of polyhydride compounds of tungsten, rhenium, osmium, and iridium react with HBF_4 in acetonitrile to form molecular hydrogen and solvated complexes.[18] Recently, Tilset

(7) (a) Antiñolo, A.; Chaudret, B.; Commenges, G.; Fajardo, M.; Jalón, F.; Morris, R. H.; Otero, A.; Schweltzer, C. T. *J. Chem. Soc., Chem. Commun*. **1988**, 1210. (b) Heinekey, D. M. *J. Am. Chem. Soc*. **1991**, *113*, 6074. (c) Barthelat, J. C.; Chaudret, B.; Daudey, J. P.; De Loth, Ph.; Poilblanc, R. *J. Am. Chem. Soc*. **1991**, *113*, 9896. (d) Antiñolo, A.; Carrillo, F.; Fernández-Baeza, J.; Otero, A.; Fajardo, M.; Chaudret, B. *Inorg. Chem*. **1992**, *31*, 5156. (e) Antiñolo, A.; Carrillo, F.; Chaudret, B.; Fajardo, M.; Fernández-Baeza, J.; Laufranchi, M.; Limbach, H. H.; Maurer, M.; Otero, A.; Pellinghelli, M. A. *Inorg. Chem*. **1994**, *33*, 5163.

(8) (a) Arliguie, T.; Border, C.; Chaudret, B.; Devillers, J.; Poilbanc, R. *Organometallics* **1989**, *8*, 1308. (b) Heinekey, D. M.; Payne, N. G.; Sofield, C. D. *Organometallics* **1990**, *9*, 2643. (c) Arliguie, T.; Chaudret, B.; Jalon, F., Otero, A.; López, J. A.; Lahoz, F. J. *Organometallics* **1991**, *10*, 1888.

(9) (a) Heinekey, D. M.; Harper, T. G. P. *Organometallics* **1991**, *10*, 2891. (b) Gusev, D. G.; Kuhlman, R.; Sini, G.; Eisenstein, O.; Caulton, K. G. *J. Am. Chem. Soc*. **1994**, *116*, 2685. (c) Kuhlman, R.; Clot, E.; Leforestier, C.; Streib, W. E.; Eisenstein, O.; Caulton K. G. *J. Am. Chem. Soc*. **1997**, *119*, 10153.

(10) (a) Heinekey, D. M.; Payne, N. G.; Schulte, G. K. *J. Am. Chem. Soc*. **1988**, *110*, 2303. (b) Zilm, K. W.; Heinekey, D. M.; Millar, J. M.; Payne, N. G.; Demou, P. *J. Am. Chem. Soc*. **1989**, *111*, 3088. (c) Heinekey, D. M.; Millar, J. M.; Koetzle, T. F.; Payne, N. G.; Zilm, K. W. *J. Am. Chem. Soc*. **1990**, *112*, 909. (d) Heinekey, D. M.; Hinkle, A. S.; Close, J. D. *J. Am. Chem. Soc*. **1996**, *118*, 5353.

(11) (a) Jones, D. H.; Labinger, J. A.; Weitekamp, D. P. *J. Am. Chem. Soc*. **1989**, *111*, 3087. (b) Jarid, A.; Moreno, M.; Lledós, A.; Lluch, J. M.; Bertrán, J. *J. Am. Chem. Soc*. **1993**, *115*, 5861. (c) Zilm, K. W.; Heinekey, D. M.; Millar, J. M.; Payne, N. G.; Neshyba, S. P.; Duchamp, J. C.; Szczyrba, J. *J. Am. Chem. Soc*. **1990**, *112*, 920.

(12) Limbach, H. H.; Scherer, G.; Maurer, M.; Chaudret, B. *Angew. Chem., Int. Ed. Engl*. **1992**, *31*, 1369.

(13) Clot, E.; Leforestier, C.; Eisenstein, O.; Pélissier, M. *J. Am. Chem. Soc*. **1995**, *117*, 1797.

(14) (a) Esteruelas, M. A.; Jean, Y.; Lledós, A.; Oro, L. A.; Ruiz, N.; Volatron, F. *Inorg. Chem*. **1994**, *33*, 3609. (b) Buil, M. L.; Espinet, P.; Esteruelas, M. A.; Lahoz F. J.; Lledós, A.; Martínez-Ilarduya, J. M.; Maseras, F.; Modrego, J.; Oñate, E.; Oro, L. A.; Sola, E.; Valero, C. *Inorg. Chem*. **1996**, *35*, 1250. (c) Esteruelas, M. A.; Lahoz, F. J.; López, A. M.; Oñate, E.; Oro, L. A.; Ruiz, N.; Sola, E.; Tolosa, J. I. *Inorg. Chem*. **1996**, *35*, 7811. (d) Castillo, A.; Esteruelas, M. A.; Oñate, E.; Ruiz, N. *J. Am. Chem. Soc*. **1997**, *119*, 9691. (e) Barea, G.; Esteruelas, M. A.; Lledós, A.; López, A. M.; Oñate, E.; Tolosa, J. I. *Organometallics* **1998**, *17*, 4065.

(15) (a) Bader, R. F. W. *Atoms in Molecules: A Quantum Theory*; Oxford University Press: New York 1990. (b) Bader, R. F. W. *Chem. Rev*. **1991**, *91*, 893.

(16) (a) Lin, Z.; Hall, M. B. *Inorg. Chem*. **1992**, *31*, 4262. (b) Lin, Z.; Hall, M. B. *Organometallics* **1993**, *12*, 4046.

(17) Maseras, F.; Lledós, A.; Costas, M.; Poblet, J. M. *Organometallics* **1996**, *15*, 2947.

(18) Crabtree, R. H.; Hlatky, G. G.; Parnell, C. P.; Segmüller, B. E.; Uriarte, R. J. *Inorg. Chem*. **1984**, *23*, 354.

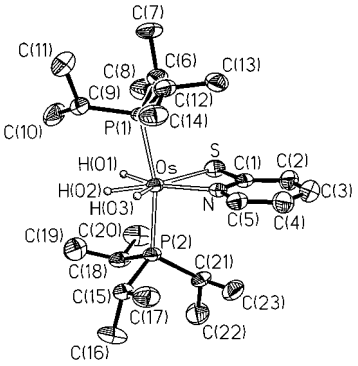

Figure 1. Molecular diagram of the complex $OsH_3\{\kappa\text{-}N,\kappa\text{-}S\text{-}(2\text{-Spy})\}(P^iPr_3)_2$ (**2**). Thermal ellipsoids are shown at 50% probability.

Table 1. Selected Bond Lengths (Å) and Angles (deg) for the Complex $OsH_3\{\kappa\text{-}N,\kappa\text{-}S\text{-}(2\text{-Spy})\}(P^iPr_3)_2$ (**2**)

Os−P(1)	2.336(2)	H(02)···H(03)	1.62(9)
Os−P(2)	2.347(2)	N−C(1)	1.354(7)
Os−S	2.513(2)	C(1)−C(2)	1.404(7)
Os−N	2.148(4)	C(2)−C(3)	1.373(9)
Os−H(01)	1.61(8)	C(3)−C(4)	1.407(8)
Os−H(02)	1.50(6)	C(4)−C(5)	1.352(7)
Os−H(03)	1.51(7)	N−C(5)	1.350(7)
H(01)···H(02)	1.4(1)		
P(1)−Os−P(2)	165.76(5)	S−Os−N	65.7(1)
P(1)−Os−S	95.16(5)	S−Os−H(01)	90(3)
P(1)−Os−N	97.8(1)	S−Os−H(02)	145(2)
P(1)−Os−H(01)	81(2)	S−Os−H(03)	150(3)
P(1)−Os−H(02)	85(2)	N−Os−H(01)	156(3)
P(1)−Os−H(03)	85(2)	N−Os−H(02)	149(2)
P(2)−Os−S	94.71(5)	N−Os−H(03)	84(2)
P(2)−Os−N	95.7(1)	H(01)−Os−H(02)	55(4)
P(2)−Os−H(01)	89(2)	H(01)−Os−H(03)	119(4)
P(2)−Os−H(02)	81(2)	H(02)−Os−H(03)	65(3)
P(2)−Os−H(03)	92(2)		

and Caulton[19] have also investigated the protonation of **1** with HBF_4, which leads to the cationic dihydrogen complex $[OsH_3(\eta^2\text{-}H_2)_2(P^iPr_3)_2]^+$. In acetonitrile, the nitrogen donor ligand displaces the two dihydrogen ligands to give $[OsH_3(NCCH_3)_2(P^iPr_3)_2]^+$.

In the solid state, the structure of **2** was determined by an X-ray crystallographic study. The structure of the molecule is presented in Figure 1. Selected bond distances and angles are listed in Table 1.

The coordination geometry around the osmium atom can be rationalized as a distorted pentagonal bipyramid with the two phosphorus atoms of the triisopropylphoshine ligands occupying axial positions [P(1)−Os−P(2) = 165.76(5)°]. The osmium coordination sphere is completed by the hydride ligands, which were located in the final Fourier difference map and refined in the final steps of refinement, and the nitrogen and sulfur atoms of the pyridine-2-thiolato group, which acts with a bite angle of 65.7(1)°, which is a similar value to that reported for the complex $[Os\{\kappa\text{-}N,\kappa\text{-}S\text{-}(2\text{-Spy})\}(\eta^2\text{-}H_2)(CO)(PPh_3)_2]BF_4$ [67.3(3)°][20] and related ruthenium compounds.[21] The Os−S and Os−N bond lengths are 2.513(2) and 2.148(4) Å, respectively. The hydride ligands are roughly coplanar with the osmium atom and form the triangle shown in Figure 2.

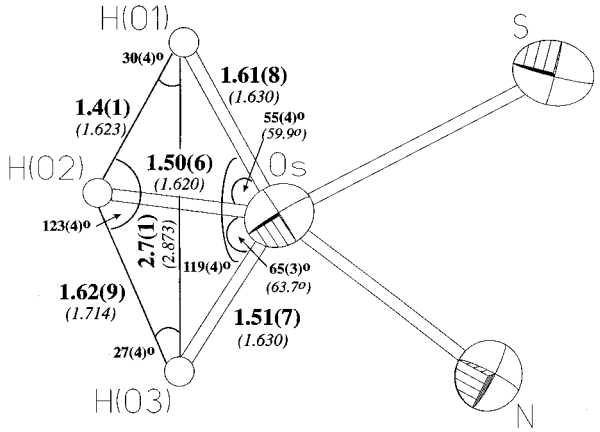

Figure 2. Geometry of the OsH_3 unit in $OsH_3\{\kappa\text{-}N,\kappa\text{-}S\text{-}(2\text{-Spy})\}(P^iPr_3)_2$ (**2**) from X-ray determination (bold) and from theoretical determination (italic).

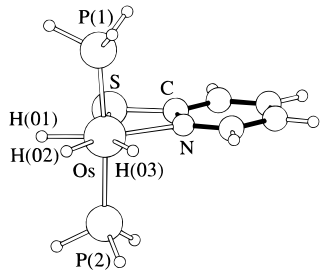

2a

Figure 3. Optimized structure of the $OsH_3\{\kappa\text{-}N,\kappa\text{-}S\text{-}(2\text{-Spy})\}(PH_3)_2$ complex **2a**.

2. Nature of the OsH_3 Unit. In general, the M−H distances obtained from X-ray diffraction data are imprecise.[22] However, ab initio calculations have been shown to provide useful, accurate data for the hydrogen positions in both classical polyhydride[6,14,23a,b] and nonclassical dihydrogen complexes.[17,23c−f] In light of this we have performed a theoretical structural determination of **2** taking the complex $OsH_3\{\kappa\text{-}N,\kappa\text{-}S\text{-}(2\text{-Spy})\}(PH_3)_2$ (**2a**) as the model. The optimized geometry of **2a** is depicted in Figure 3, and its main geometrical parameters are collected in Table 2.

In agreement with the X-ray structure of **2**, the geometry of **2a** can best be described as a pentagonal bipyramid. The main discrepancy between the two is found in the P−Os−P bond angle [175.1° versus 165.76(5)°] and is probably due to the substitution of the bulky triisopropylphosphine ligand by phosphine. The Os−H distances, H−Os−H angles, and hydrogen−hydrogen separations (Figure 2) are consistent with the trihydride nature of the complex. In this context, it should be mentioned that all attempts to obtain a minimum with a dihydrogen structure have led to the trihydride minimum.

The geometry of the OsH_3 unit resembles that proposed from spectroscopic data and theoretical calculations for the complexes $OsH_3X(P^iPr_3)_2$ (X = Cl, Br, I).[9b] In these compounds the OsH_3 unit adopts a C_{2v} structure. However, the presence of the

(19) Smith, K. T.; Tilset, M.; Kuhlman, R.; Caulton, K. G. *J. Am. Chem. Soc.* **1995**, *117*, 9473.
(20) Schlaf, M.; Lough, A. J.; Morris, R. H. *Organometallics* **1993**, *12*, 3808.
(21) Mura, P.; Olby, B. G.; Robinson, S. D. *J. Chem. Soc., Dalton Trans.* **1985**, 2101 and references therein.
(22) Zhao, D.; Bau, R. *Inorg. Chim. Acta* **1998**, *269*, 162.
(23) (a) Lin, Z.; Hall, M. B. *Inorg. Chem.* **1991**, *30*, 2569. (b) Lin, Z.; Hall M. B. *Coord. Chem. Rev.* **1994**, *135*, 845. (c) Dapprich, S.; Frenking, G. *Angew. Chem., Int. Ed. Engl.* **1995**, *34*, 354. (d) Bakhmutov, V. I.; Bertrán, J.; Esteruelas, M. A.; Lledós, A.; Maseras, F.; Modrego, J.; Oro, L. A.; Sola, E. *Chem. Eur. J.* **1996**, *2*, 815. (e) Gelabert, R.; Moreno, M.; Lluch, J. M.; Lledós, A. *Organometallics* **1997**, *16*, 3805. (f) Albéniz, M. J.; Esteruelas, M. A.; Lledós, A.; Maseras, F.; Oñate, E.; Oro, L. A.; Sola, E.; Zeier, B. *J. Chem. Soc., Dalton Trans.* **1997**, 181.

Table 2. Selected Bond Lengths (Å) and Angles (deg) for the B3LYP Optimized Structures of the $OsH_3\{\kappa\text{-}N,\kappa\text{-}S\text{-}(2\text{-}Spy)\}(PH_3)_2$ System

	2a	2a-TStN	2a-TStS
Os−H(01)	1.630	1.721	1.639
Os−H(02)	1.620	1.721	1.690
Os−H(03)	1.630	1.632	1.690
Os−P	2.328	2.337	2.335
Os−N	2.177	2.112	2.224
Os−S	2.597	2.645	2.513
H(01)−H(02)	1.623	0.894	2.310
H(02)−H(03)	1.714	2.347	0.957
H(01)−Os−H(02)	59.9	30.1	87.9
H(02)−Os−H(03)	63.7	88.8	32.9
H(01)−Os−S	85.3	106.7	103.9
H(01)−Os−N	150.1	106.7	169.7
H(02)−Os−S	145.2	106.7	159.9
H(02)−Os−N	150.0	163.1	102.0
H(03)−Os−S	151.2	164.0	159.9
H(03)−Os−N	86.3	99.2	102.0
N−Os−S	64.9	64.8	65.8
P−Os−P	175.1	173.1	163.1

asymmetric pyridine-2-thiolato ligand in **2a** produces a loss of symmetry. Thus, although there are only two different Os−H distances (1.63 Å for both terminal Os−H bonds and 1.62 Å for the central Os−H bond) a more detailed inspection of the ligand positions in the equatorial plane reveals the asymmetry in the position of the central hydride H(02). The H(02)−Os−S and H(02)−Os−N angles are clearly different (145.2° and 150.0°, respectively) indicating that H(02) is closer to the hydride cis to the S atom [H(02)−H(01) = 1.623 Å] than to the hydride cis to the N atom [H(02)−H(03) = 1.714 Å].

To further elucidate the nature of the M−H interactions in the trihydride structure, we have performed a topological analysis of the electron density in **2a**, on the basis of Bader's atoms in molecules theory (AIM). Figure 4 presents the electron density (Figure 4a) and the Laplacian (Figure 4b) plots in the plane defined by the metal and the three hydride ligands. The regions of charge concentration are represented by dashed lines. An indicative bond structure is also presented in this Figure.

The AIM scheme is based on the topological properties of the electron density $\rho(r)$ which are summarized in terms of its critical points (cp) [points where $\nabla\rho(r_{cp}) = 0$].[15] The Laplacian of the charge density $\nabla^2\rho(r)$ is defined as the sum of the three principal curvatures of the ρ function in each point in space. A critical point (cp) is characterized by the sign of its curvatures. The nuclear positions correspond to local maxima in the electron density and are zero-gradient points with three negative eigenvalues: (3, −3) cp. A bond critical point is a (3, −1) cp. It exhibits one positive (minimum in one direction) and two negative (maximum in two directions) eigenvalues. A ring critical point is a (3, +1) cp. It presents two positive curvatures in the ring surface and a negative curvature along an axis perpendicular to the ring surface. In turn, the sign of the Laplacian of charge density determines whether the electronic charge is locally concentrated [$\nabla^2\rho(r) < 0$] or depleted ($\nabla^2\rho(r) > 0$). A negative value of the Laplacian of the charge density at a bond critical point is related to a covalent bond, showing a sharing of charge. Positive values are characteristic of "closed-shell" interactions such as ionic bonds.

The electron density plot of **2a** shows only three bond critical points corresponding to three M−H bonds and no bond critical point connecting the hydrogen atoms. The map of the Laplacian plot of ρ computed for **2a** exhibits three separated charge concentrations associated with each hydride ligands. Table 3 collects the bond properties obtained for the M−H bonds in complex **2a**. The values of ρ_{cp} (charge density of the critical point) and $\nabla^2\rho_{cp}$ (sum of the three curvatures of the Hessian matrix at the critical point) for the Os−H bonds are very close to that calculated for $OsH_4(PH_3)_3$,[17] an example of a well-characterized polyhydride complex with nonbonded cis hydride ligands.[24] Values of $\nabla^2\rho_{cp}$ at the three bond critical points indicate that the three Os−H bonds are slightly different from an electronic point of view. We have computed the atomic

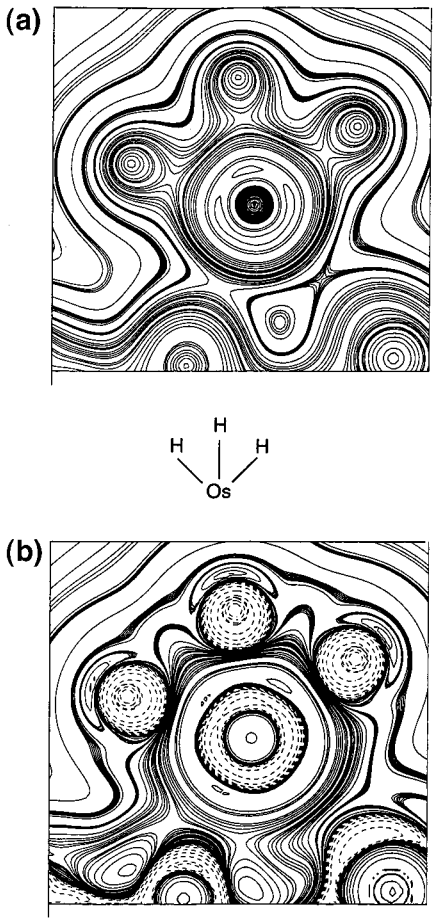

Figure 4. (a) Electron isodensity contour plot of the minimum **2a**. (b) Plot of $\nabla^2\rho$ for complex **2a**. Solid lines are for $\nabla^2\rho > 0$ (regions of charge depletion); dashed lines are for $\nabla^2\rho < 0$ (regions of charge concentration).

Table 3. Bond Properties of the H−H and M−H Bonds of the Stationary Points of $OsH_3\{\kappa\text{-}N,\kappa\text{-}S\text{-}(2\text{-}Spy)\}(PH_3)_2$ System[a]

complex	bond	type	ρ_{cp}	$\Delta^2_{\rho cp}$	bond length[b]
2a	Os−H(01)	(3, −1)	0.142	+0.082	1.630
	Os−H(02)	(3, −1)	0.145	+0.066	1.620
	Os−H(03)	(3, −1)	0.142	+0.092	1.630
2a-TStN	Os−H(01)	(3, −1)	0.101	+0.332	1.721
	Os−H(02)	(3, −1)	0.101	+0.332	1.721
	Os−H(03)	(3, −1)	0.136	+0.166	1.632
	H(01)−H(02)	(3, −1)	0.194	−0.503	0.894
	H(01)−Os−H(02)	(3, +1)	0.098	+0.470	
2a-TStS	Os−H(01)	(3, −1)	0.139	+0.129	1.639
	Os−H(02)	(3, −1)	0.117	+0.309	1.690
	Os−H(03)	(3, −1)	0.117	+0.309	1.690
	H(02)−H(03)	(3, −1)	0.192	−0.487	0.957
	H(02)−Os−H(03)	(3, +1)	0.111	+0.368	

[a] Atomic units: for ρ, 1 au = e/a_0^3 = 6.748 e Å^{-3}; for $\Delta^2\rho$, 1 au = e/a_0^5 = 24.10 e Å^{-5}. [b] In Å.

(24) Hart, D. W.; Bau, R.; Koetzle, T. F. *J. Am. Chem. Soc.* **1997**, *99*, 7557.

charges for the three hydrogen atoms by integration of the charge density over the atomic domain. In agreement with the trihydride nature of the complex the Bader net charges are negative, but the charge which each hydride bears is different: −0.22 e H(01), −0.16 e H(02), and −0.24 e H(03). In the site cis to the N atom less electronic density is transferred from the ligand to the metal. The more ionic character of the Os−H(03) bond can also be inferred from the more positive value of the $\nabla^2\rho$ at the corresponding critical point.

3. Thermally Activated Site Exchange Processes in the OsH_3 Unit. At room temperature the $^{31}P\{^1H\}$ NMR spectrum of **2** shows a singlet at 24.0 ppm, which is split into a quartet, as a result of the coupling with three hydride ligands. The signal for the hydride ligands in the ^1H NMR spectrum appears at −11.53 ppm as a 1:2:1 triplet with a H−P coupling constant of 12.8 Hz. In the low-field region, the spectrum shows the characteristic resonances of the isopropyl protons of the phosphine and those corresponding to the inequivalent protons of the pyridine-2-thiolato ligand at 8.12, 6.60, 6.51, and 6.20 ppm. We have assigned the resonance at the lowest field to the proton ortho to the nitrogen atom of the chelate ligand on the basis of a NOE experiment. Irradiation of the hydride resonance gave an increase (13.8%) in the intensity of the resonance at 8.12 ppm, while a NOE effect was not observed with the resonances close to 6 ppm.

The $^{31}P\{^1H\}$ NMR spectrum in toluene-d_8/dichloromethane-d_2 (1:1) is temperature invariant between 305 and 175 K. However, the ^1H NMR spectrum is temperature dependent. Lowering the sample temperature leads to broadening of the hydride resonance. Between 245 and 235 K, a first decoalescence occurs and, at lower temperature, a second one. At 175 K an $ABCX_2$ spin system (X = ^{31}P) is observed, which is simplified to the expected ABC spin system in the $^1H\{^{31}P\}$ NMR spectrum (Figure 5), where the values of the chemical shift and the H−H coupling constants are −10.80 (A), −11.60 (B), and −12.05 ppm (C) and 0.0 (J_{AB}), 9.3 (J_{BC}), and 32.6 Hz (J_{AC}), respectively.

To fit the hydride resonances to the hydride ligands of **2**, we carried out a ROESY ^1H NMR experiment, at 173 K. As a result of this experiment (Figure 6), we assigned the resonance B to H(03). In addition the resonances C and A were assigned to the hydrides H(02) and H(01), respectively, on the basis of the values of the J_{AB}, J_{BC}, and J_{AC} coupling constants.

The spectra of Figure 5 are consistent with the operation of two thermally activated site exchange processes. Line shape analysis of these spectra allows the calculation of the rate constants for both thermal exchange processes at different temperatures. The activation parameters obtained from the Eyring analysis are $\Delta H^{\ddagger}$ = 8.9 (±0.2) kcal mol^{-1} and $\Delta S^{\ddagger}$ = −2.2 (±0.6) cal K^{-1} mol^{-1} for the H(02)−H(03) exchange and $\Delta H^{\ddagger}$ = 10.2 (±0.3) kcal mol^{-1} and $\Delta S^{\ddagger}$ = −3 (±2) cal K^{-1} mol^{-1} for the H(01)−H(02) exchange.

To find the transition states for these processes, theoretical calculations were carried out. The transition states [**2a-TStN** for the H(01)−H(02) exchange, and **2a-TStS** for the H(02)−H(03) exchange] were calculated by a Cs-restricted geometry optimization with H(01) and H(02) (**2a-TStN**) and H(02) and H(03) (**2a-TStS**) twisted 90° with respect to the position of the minimum in **2a**. The structures calculated by this method are depicted in Figure 7. Selected bond distances and angles are collected in Table 2 (second and third columns).

Both transition states have a η^2-H_2 complex-like nature. This observation comes from the hydrogen−hydrogen distances and H−Os−H angles between the exchanging atoms (0.894 Å and 30.1° in **2a-TStN** and 0.957 Å and 32.9° in **2a-TStS**). Their geometries are nearly octahedral with H(03)−Os−X and N−Os−X angles of 88.7° and 172.1°, respectively, in **2a-TStN** and H(01)−Os−X and S−Os−X angles of 87.8° and 168.2°, respectively, in **2a-TStS** (X = midpoint of the H−H segment of the dihydrogen). Thus, both transition states can be described as d^6 six-coordinate Os(II) species containing a dihydrogen ligand, which is trans to the nitrogen atom in **2a-TStN**, and trans to the sulfur atom in **2a-TStS**. In agreement with this geometrical similarity, the activation barriers for the two

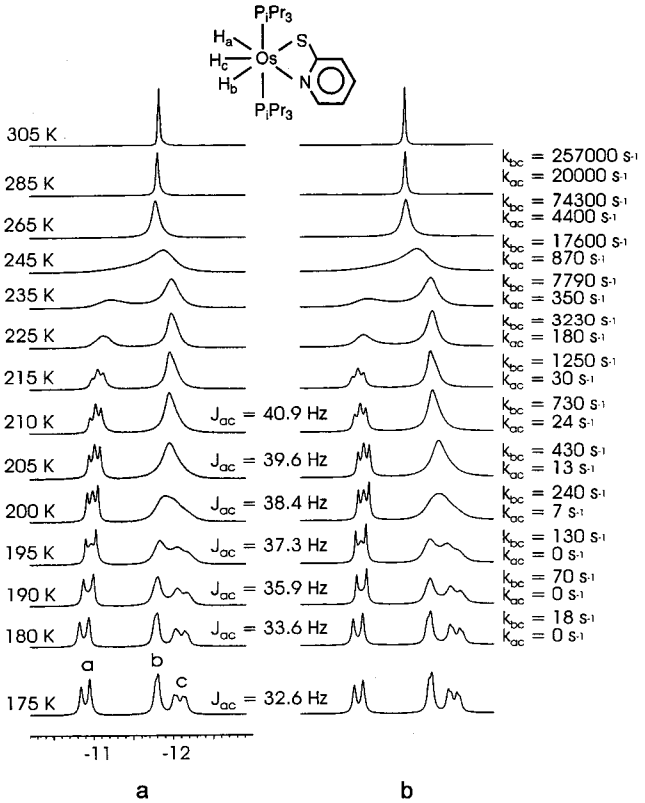

Figure 5. (a) Variable temperature $^1H\{^{31}P\}$ NMR spectra (300 MHz) in C_7D_8/CD_2Cl_2 (1:1) in the high-field region of $OsH_3\{\kappa$-*N*,κ-*S*-(2-Spy)$\}$-(P^{i}Pr$_3$)$_2$ (**2**). (b) Simulated spectra. J_{ac}, temperatures, and rate constants for the intramolecular hydrogen site-exchange process are also provided.

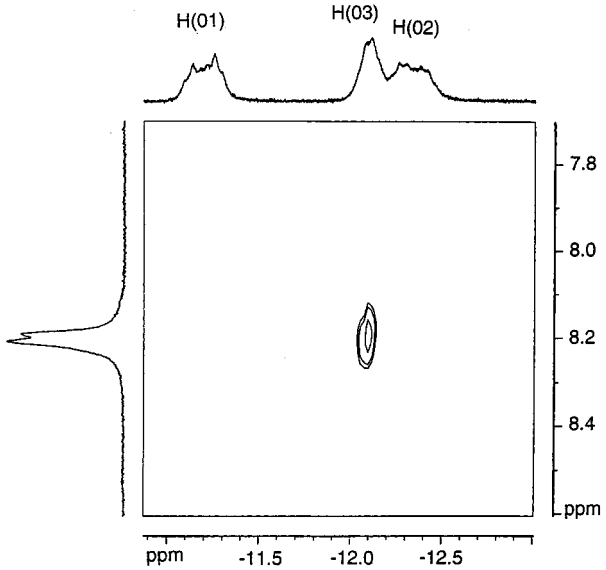

Figure 6. Partial view of the ROESY ^1H NMR spectrum at 173 K in C_7D_8/CD_2Cl_2 (1:2) of $OsH_3\{\kappa$-*N*,κ-*S*-(2-Spy)$\}$(P^{i}Pr$_3$)$_2$ (**2**).

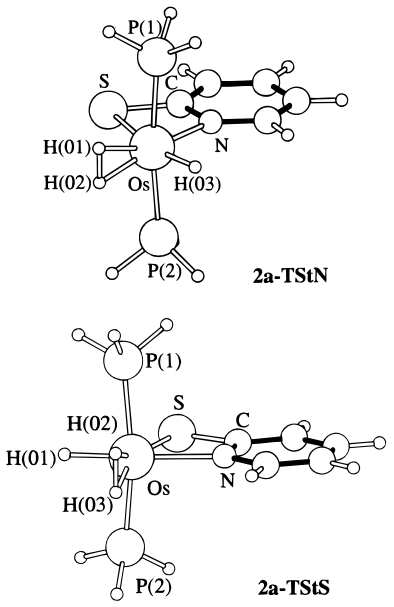

Figure 7. Transition state structures for the hydrogen exchange processes in the $OsH_3\{\kappa\text{-}N,\kappa\text{-}S\text{-}(2\text{-}Spy)\}(PH_3)_2$ system: (a) **2a-TStN**; (b) **2a-TStS**.

exchange processes are similar, 14.9 kcal mol^{-1} for the H(01)−H(02) exchange and 16.2 kcal mol^{-1} for the H(02)−H(03) exchange. These values are slightly higher than those calculated by NMR spectroscopy. The discrepancy is probably due to the substitution of the bulky triisopropylphosphine by phosphine in the model and/or solvent effects.

The comparison of the transition states and **2a** shows noticeable variations in the Os−N and Os−S distances. The weaker trans influence of the dihydrogen ligand with regard to the hydride ligand produces a shortening of the bond distances trans to the dihydrogen [Os−N in **2a-TStN** (2.112 versus 2.177 Å) and Os−S in **2a-TStS** (2.513 versus 2.597 Å)]. A similar effect on the Os−N distances has been observed in the X-ray data of the complexes *trans*-$[OsH(CH_3CN)(dppe)_2]BF_4$ (2.109 Å) and *trans*-$[Os(\eta^2\text{-}H_2)(CH_3CN)(dppe)_2][BF_4]_2$ (2.079 and 2.066 Å).[25] On the contrary, the stronger trans influence in the transition states of the remaining hydride ligand provokes a lengthening of the metal−ligand bond trans to the hydride.

To further elucidate the nature of the M−H interactions in the transition states, we have also performed a topological analysis of the electron density in **2a-TStN** and **2a-TStS**, on the basis of Bader's atoms in molecules theory. Because the results of the topological analysis of the electron density in both transition states are very similar (Table 3), we will focus our discussion on **2a-TStN**. The electron density plot of **2a-TStN** in the plane defined by the metal and the two exchanging hydrogens [H(01) and H(02)] is depicted in Figure 8a, and the Laplacian plot is presented in Figure 8b. The density map of **2a-TStN** is sharply different from that of the minimum **2a** (Figure 4a). In the transition state there is a clear bond path between H(01) and H(02), characteristic of a dihydrogen complex. Accordingly, a bond critical point can be found between H(01) and H(02) with a negative value of $\nabla^2\rho_{cp}$, typical of a covalent bond. In addition, a ring critical point (3, +1) appears between the two exchanging hydrogens and the metal. The distribution of the $\nabla^2\rho$ shows a region of charge concentration around the dihydrogen ligand. Such an electron density

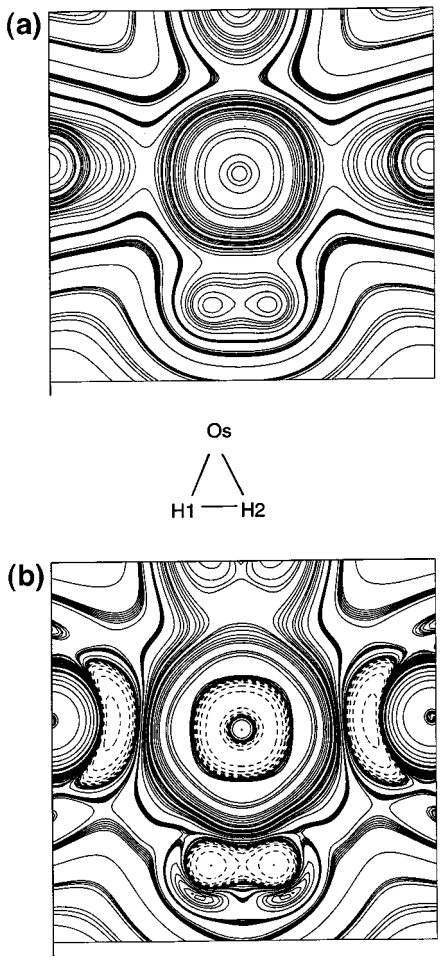

Figure 8. (a) Electron isodensity contour plot of the transition state **2a-TStN**. (b) Plot of $\nabla^2\rho$ for complex **2a-TStS**. Solid lines are for $\nabla^2\rho > 0$ (regions of charge depletion); dashed lines are for $\nabla^2\rho < 0$ (regions of charge concentration).

concentration between two hydrogens has been reported for nonclassical dihydrogen complexes.[16,17] The Bader net charges are also consistent with the dihydrogen−hydride nature of the transition state. The charges of H(01) and H(02) have diminished to −0.05 e, whereas H(03) bears a charge of −0.29 e. The increase of the negative charge on the hydride ligand in the transition state with respect to that in the minimum, together with its placement in a more directly trans position with respect to the sulfur atom, are responsible for the stronger trans influence of the hydride in the transition state. In agreement with the change in the formal oxidation state of the metal, the charge on the osmium atom changes from +0.81 e in the minimum to +0.62 e in the transition state.

4. T_1(min) Values of the OsH_3 Unit. The T_1 values of hydrogen nuclei of the OsH_3 unit were determined over the temperature range 265−175 K. The T_1(min) values were found at the same temperature (205 K) when the ^1H NMR spectrum shows a double triplet for H(01) and a broad resonance for both H(02) and H(03) (as a result of the thermal exchange processes H(01)−H(02) and H(02)−H(03) with rate constants of 13 and 430 s^{-1}, respectively). These values are 92 ms for H(01) and 74 ms for H(02)/H(03).

T_1(min) values for polyhydride complexes can be calculated from internuclear distances obtained from neutron and X-ray diffraction studies[26] and theoretical calculations.[14a] To test the hydrogen−hydrogen separations obtained for **2a**, we have estimated the T_1(min) values for the hydrogen nuclei of the OsH_3

(25) Schlaf, M.; Lough, A. J.; Maltby, P. A.; Morris, R. H. *Organometallics* **1996**, *15*, 2270.

Table 4. Coupling Constants as a Function of Temperature for $OsH_3\{\kappa\text{-}N,\kappa\text{-}S\text{-}(2\text{-}Spy)\}(P^iPr_3)_2$ (**2**)

T (K)	J_{obs} (Hz)	J_{ex} (Hz)
175	32.6	−3.8
180	33.6	−4.3
190	35.9	−5.5
195	37.3	−6.2
200	38.4	−6.7
205	39.6	−7.3
210	40.9	−8.0

unit of **2**, assuming H(01)−H(02) and H(02)−H(03) separations of 1.623 and 1.714 Å, respectively.

The total relaxation rate for H_n ($R_n = 1/T_1(\text{min})$ (H_n)) is the addition of the relaxation rate due to the hydride dipole−dipole interactions (at 300 MHz $R_{H-H} = 129.18/r_{(H-H)}^6$) and that due to all other relaxation contributors (R^*).[1c] Thus, one can obtain values of T_1(min) converted to the 300 MHz scale for each hydride ligand by using eqs 3−5, since R^* can be estimated to be 5.2 s^{-1} the average value of those found in the osmium trihydrides $[OsH_3(\text{diolefin})(P^iPr_3)_2]BF_4$ (diolefin = NBD, TFB).[14d]

$$R_{H(01)} = R^* + R_{H(01)-H(02)} + R_{H(01)-H(03)} \quad (3)$$

$$R_{H(02)} = R^* + R_{H(01)-H(02)} + R_{H(02)-H(03)} \quad (4)$$

$$R_{H(03)} = R^* + R_{H(02)-H(03)} + R_{H(01)-H(03)} \quad (5)$$

Furthermore, above exchange rates of about 100 s^{-1}, the relaxation rate is the weighted average of the relaxation rate for each type of hydride.[26] So, it is also possible to calculate a relaxation rate for the H(02)/H(03) resonance at 205 K by using eq 6.

$$R = (R_{H(02)} + R_{H(03)})/2 \quad (6)$$

Solving $R_{H(01)}$ and R yields values of 12.5 and 14.0 s^{-1}, which lead to T_1(min) values of 80 and 71 ms, respectively, which are in good agreement with those determined by NMR spectroscopy (92 and 74 ms).

5. Quantum Exchange Process in the OsH_3 Unit. The values of the chemical shifts of the H(01), H(02), and H(03) sites as well as the H(01)−H(02) and H(02)−H(03) coupling constants show no significant temperature dependence. However, the magnitude of the observed H(01)−H(02) coupling constant is sensitive to temperature, increasing from 32.6 to 40.9 Hz as the temperature is increased from 175 to 210 K (Table 4). This can be readily explained in terms of the quantum exchange coupling between H(01) and H(02).

Recently, as an expansion of their previous work, Heinekey and co-workers have reported an adaptation of the Landesman results from the work done on the $^3He/^4He$ system.[10d] In this adapted model, for a given temperature, J_{ex} is determined by three parameters characteristic for each compound, which are considered temperature invariant: a, ν, and λ (eqs 7 and 8).

$$J_{ex} = (-\hbar a/2m\pi^2\lambda\delta^2)\exp\{-(a^2+\lambda^2)/2\delta^2\} \quad (7)$$

$$\delta^2 = [h/4\pi^2 m\nu]\coth[h\nu/2kT] \quad (8)$$

Parameter a is the internuclear distance between the hydride ligands, ν is believed to describe the H−M−H vibrational wag mode which allows movement along the H−H internuclear vector, and λ is the hard sphere radius of the hydrogens.

(26) Desrosiers, P. J.; Cai, L.; Lin, Z.; Richards, R.; Halpern, J. *J. Am. Chem. Soc.* **1991**, *113*, 4173.

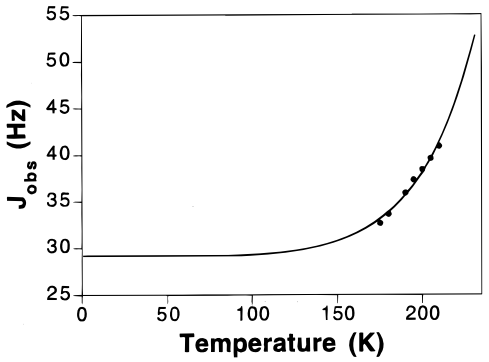

Figure 9. Plot of the fit of the J_{obs} versus temperature data for **2**.

Although this model suffers from several approximations, from an experimental point of view it has the advantage of allowing a straightforward quantification. Thus, by combining eqs 1, 7, and 8, one obtains eq 9 where, for a given internuclear distance and a given temperature, J_{obs} is determined by J_{mag}, λ, and ν.[14d]

$$J_{obs} = J_{mag} + 2[(2\nu\hbar a/\lambda h\coth[h\nu/2kT]) \times \exp\{-2\pi^2 m\nu(a^2+\lambda^2)/h\coth[h\nu/2kT]\}] \quad (9)$$

Accepting a value for the H(01)−H(02) separation of 1.623 Å (that found for **2a**), the plot of the fit of the $J_{H(01)H(02)} = J_{obs}$ versus temperature (Figure 9) indicates that the temperature dependence phenomenon fits into the 2D harmonic oscillator model represented by eq 9. The parameters obtained from the computer fitting are $J_{mag} = 25$ Hz, $\lambda = 1.0$ Å, and $\nu = 538$ cm^{-1}. The determined value of J_{mag} was then used to calculate the values of the corresponding J_{ex} at each temperature (Table 4), according to eq 1.

The values of J_{mag}, λ, and ν agree well with those previously found for complexes of the types $[OsH_3(\text{diolefin})(P^iPr_3)_2]^+$,[14d] $IrH_3(\eta^5\text{-}C_5H_5)(PR_3)$, and $IrH_3(\eta^5\text{-}C_5Me_5)(PR_3)$.[10d]

6. Other $OsH_3(\kappa\text{-}X,\kappa\text{-}Y\text{-}XYR)(P^iPr_3)_2$ Systems. Similarly to the reaction of **1** with pyridine-2-thiol to afford **2**, the treatment of **1** with L-valine or 2-hydroxy-pyridine in a 1:1 molar ratio, in refluxing toluene, gives the complexes $OsH_3\{\kappa\text{-}N,\kappa\text{-}O\text{-}OC(O)CH[CH(CH_3)_2]NH_2\}(P^iPr_3)_2$ (**3**) and $OsH_3\{\kappa\text{-}N,\kappa\text{-}O\text{-}(2\text{-}Opy)\}(P^iPr_3)_2$ (**4**), respectively (eq 10), which were isolated as white (**3**) and yellow (**4**) solids in 90% (**3**) and 65% (**4**) yield.

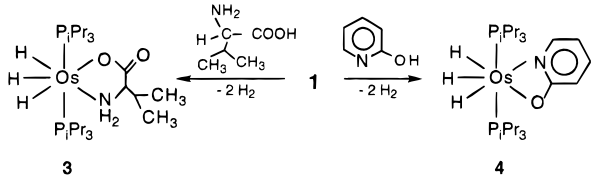

(10)

In agreement with the mutually trans disposition of the phosphine ligands, the $^{31}P\{^1H\}$ NMR spectrum of **3**, at room temperature and in dichloromethane-d_2 as solvent, shows an AB spin system centered at 31.3 ppm, with a P−P coupling constant of 285 Hz. The $^{31}P\{^1H\}$ NMR spectrum is temperature invariant down to 200 K. However, the ^1H NMR spectrum is temperature dependent. At room temperature, the spectrum exhibits a single broad resonance in the hydride region centered at −13.9 ppm. Between 290 and 280 K, a first decoalescence occurs, and at 235 K a second one. At 200 K an ABCXX′ spin system (X = X′ = ^{31}P) is observed, which is simplified to the expected ABC spin system in the $^1H\{^{31}P\}$ NMR spectrum, where the values of the chemical shift and the H−H coupling constants are

−10.83 (A), −13.57 (B), and −14.79 (C) ppm and 10.4 (J_{AB}), 0.0 (J_{AC}), and 25.8 Hz (J_{BC}), respectively.

Although the values of the H−H coupling constants are temperature invariant, and therefore quantum exchange coupling between the hydride ligands of **3** does not occur, the NMR spectra indicate the operation of two thermally activated site exchange processes. Line shape analysis of the $^1H\{^{31}P\}$ NMR spectra allows the calculation of the rate constants for both thermal exchange processes at different temperatures. The activation parameters obtained for both processes from the corresponding Eyring analysis are very similar ($\Delta H^{\ddagger} = 11.2$ (±0.6) kcal mol^{-1} and $\Delta S^{\ddagger} = 2$ (±2) cal K^{-1} mol^{-1} for the A−B exchange and $\Delta H^{\ddagger} = 13.0$ (±0.9) kcal mol^{-1} and $\Delta S^{\ddagger} = 1$ (±2) cal K^{-1} mol^{-1} for the B−C exchange). The values for the entropy of activation and for the enthalpy of activation lie in the range found for **2** and those reported for similar thermal exchange processes in other trihydride and hydride-dihydrogen derivatives.[7−11,14,27]

To estimate the hydrogen−hydrogen separation between the hydride ligands of **3**, the T_1 values of the hydrogen nuclei of the OsH_3 unit were also determined over the temperature range 293−193 K. The T_1(min) values for the resonances of H_A (111 ms), H_B (64 ms), and H_C (78 ms) were found at the same temperature (213 K), suggesting that there is no significant influence of the thermally activated exchange processes in the observed T_1(min) values.[14d] Since the total relaxation rate is the addition of the relaxation rate due to the hydride dipole−dipole interactions and that due to all other relaxation contributors, and the later ones have been estimated as 5.2 s^{-1}, we can determine the relaxation rates due to the hydride−hydride interactions (R_{HH}) by using eqs 11−13.

$$R_{H_A} = R_{H_A-H_B} + R_{H_A-H_C} = 9.0-5.2\ s^{-1} \qquad (11)$$

$$R_{H_B} = R_{H_A-H_B} + R_{H_B-H_C} = 15.6-5.2\ s^{-1} \qquad (12)$$

$$R_{H_C} = R_{H_B-H_C} + R_{H_A-H_C} = 12.8-5.2\ s^{-1} \qquad (13)$$

Solving for $R_{H_A-H_B}$, $R_{H_B-H_C}$, and $R_{H_A-H_C}$ yields the values 3.3, 7.1, and 0.5 s^{-1}, respectively, which correspond to hydrogen−hydrogen separations of 1.8 (H_A-H_B), 1.6 (H_B-H_C), and 2.5 Å (H_A-H_C). These values indicate that the hydride ligands of the OsH_3 unit form an asymmetric triangle similar to that shown in Figure 2.

The NMR spectroscopic data of **4** are also consistent with the structure proposed for this complex in eq 10. The $^{31}P\{^1H\}$ NMR spectrum in toluene-d_8 shows a singlet at 33.2 ppm, which is temperature invariant from 295 to 180 K. However the ^1H NMR spectrum, which is similar to that of **3**, is temperature dependent. At room temperature, the spectrum exhibits a broad resonance in the hydride region centered at −12.7 ppm. Between 275 and 265 K, a first decoalescence takes place, and between 245 and 240 K a second one occurs. At 180 K an $ABCX_2$ spin system (X = ^{31}P) is observed, which is simplified to the expected ABC spin system in the $^1H\{^{31}P\}$ NMR spectrum, where the values of the chemical shifts and the H−H coupling constants are −10.12 (A), −13.32 (B), and −15.46 ppm (C) and 20.3 (J_{AB}), 23.5 (J_{BC}), and 0.0 Hz (J_{AC}), respectively.

The values of the H−H coupling constants are temperature invariant, indicating that there is no quantum exchange coupling between the hydride ligands of **4**. However, in view of the NMR spectrum, it is clear that two thermally activated site exchange processes occur. Line shape analysis of the $^1H\{^{31}P\}$ spectra

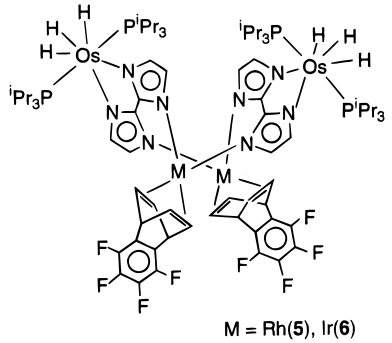

Figure 10. Structure for complexes $[(P^iPr_3)_2H_3Os(\mu\text{-biim})M(TFB)]_2$ (M = Rh (**5**), Ir (**6**)) according to all spectroscopic data.

allows the calculation of the rate constants for both thermal exchange processes at different temperatures. In this case the activation parameters obtained from the corresponding Eyring analysis are $\Delta H^{\ddagger} = 10.7$ (±0.3) kcal mol^{-1} and $\Delta S^{\ddagger} = -2.4$ (±0.8) cal K^{-1} mol^{-1} for the H_A-H_B exchange and $\Delta H^{\ddagger} = 9.8$ (±0.3) kcal mol^{-1} and $\Delta S^{\ddagger} = -3.1$ (±0.8) cal K^{-1} mol^{-1} for the H_B-H_C exchange. These values agree well with those found for compounds **2** and **3**.

The T_1 values of the hydrogen nuclei of the OsH_3 unit of **4** were determined over the temperature range 295−200 K. T_1(min) values for the H_A (88 ms), H_B (61 ms), and H_C (66 ms) resonances were found at the same temperature (215 K). From these values, we determined by a procedure similar to that previously mentioned for **3** the separations between the central hydride and those at the corners to be 1.8 and 1.6 Å, respectively.

7. The Unsymmetrical OsH_3 Unit of the Tetranuclear Complexes $[(P^iPr_3)_2H_3Os(\mu\text{-biim})M(TFB)]_2$ (TFB = Tetrafluorobenzobarrelene; M = Rh, Ir). These tetranuclear complexes [Rh (**5**), Ir (**6**)] were prepared by reaction of the trihydride $OsH_3(Hbiim)(P^iPr_3)_2$ with the dimers $[M(\mu\text{-OMe})(TFB)]_2$ (M = Rh, Ir) in boiling acetone (eq 14).

$$2OsH_3(Hbiim)(P^iPr_3)_2 + [M(\mu\text{-OMe})(TFB)]_2 \rightarrow [(P^iPr_3)_2H_3Os(\mu\text{-biim})M(TFB)]_2 + 2MeOH \quad (14)$$
(M = Rh (**5**), Ir (**6**))

The nuclearity of **5** and **6** is strongly supported by their mass spectra, which show the molecular ions centered at 1951 (**5**) and 2131 (**6**). Tetranuclear complexes containing two $[biim]^{2-}$ anions have been previously described.[28] In these molecules, each anion coordinates to the metal centers in an unsymmetrical, tetradentate manner through the four nitrogen atoms of the two imidazole rings, chelating to one metal through two nitrogens and bonding in unidentate manner to two different metal centers through the other two nitrogen atoms. In our case, this coordination bonding mode for the $[biim]^{2-}$ anions leads to molecules with C_2 symmetry (Figure 10). Thus, complexes **5** and **6** consist of two chemically equivalent $(P^iPr_3)_2H_3Os(\mu\text{-biim})M(TFB)$ units, where the phosphine and hydride ligands, and all diolefinic protons, are chemically inequivalent within

(27) (a) Earl, K. A.; Jia, G.; Maltby, P. A.; Morris, R. H. *J. Am. Chem. Soc.* **1991**, *113*, 3027. (b) Bautista, M. T.; Cappellani, E. P.; Drouin, S. D.; Morris, R. H.; Schweitzer, C. T.; Sella, A.; Zubkowski, J. *J. Am. Chem. Soc.* **1991**, *113*, 4876. (c) Jia, G.; Drouin, S. D.; Jessop, P. G.; Lough, A. J.; Morris, R. H. *Organometallics* **1993**, *12*, 906.

(28) (a) Oro, L. A.; Carmona, D.; Lamata, M. P.; Tiripicchio, A.; Lahoz, F. J. *J. Chem. Soc., Dalton Trans.* **1986**, 15. (b) Carmona, D.; Ferrer, J.; Mendoza, A.; Lahoz, F. J.; Oro, L. A.; Viguri, F.; Reyes, J. *Organometallics* **1995**, *14*, 2066.

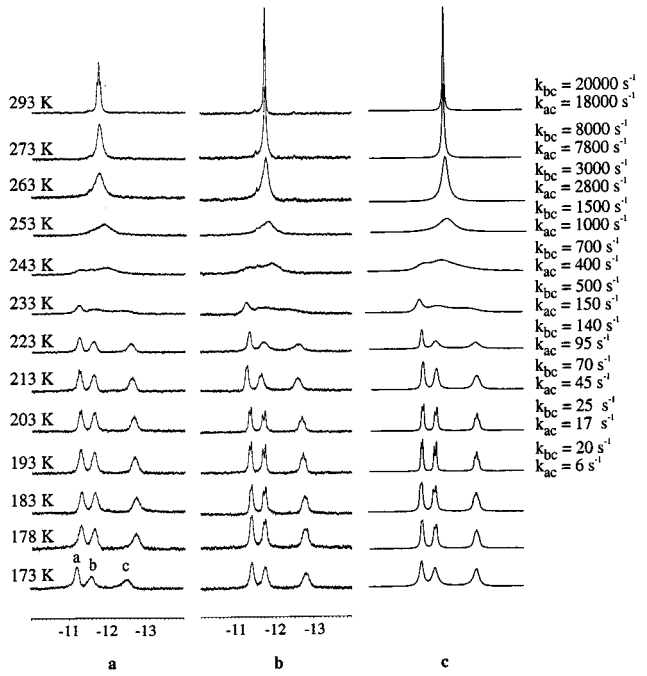

Figure 11. (a) Variable temperature ^{1}H NMR spectra (300 MHz) in CD_2Cl_2 in the high-field region of $[(P^iPr_3)_2H_3Os(\mu\text{-biim})Ir(TFB)]_2$ (**6**). (b) Observed $^1H\{^{31}P\}$ NMR (300 MHz) and simulated (c) spectra. Temperatures and rate constants (s^{-1}) for the intramolecular hydrogen site exchange process are also provided.

Table 5. $\Delta H^{\ddagger}$ (kcal mol^{-1}) and $\Delta S^{\ddagger}$ (cal K^{-1} mol^{-1}) for **5** (Rh) and **6** (Ir)

complex	$\Delta H^{\ddagger}_{ac}$	$\Delta H^{\ddagger}_{bc}$	$\Delta S^{\ddagger}_{ac}$	$\Delta S^{\ddagger}_{bc}$
5	8.0 (±0.2)	7.0 (±0.2)	−12.7 (±0.7)	−16.3 (±0.7)
6	8.7 (±0.2)	7.7 (±0.2)	−9.8 (±0.7)	−12.8 (±0.7)

each unit. In agreement with this structure, the low temperature ^{1}H NMR spectra of **5** and **6** show six resonances for the protons of the diolefin and three resonances [ABCXY spin system (X = Y = ^{31}P)] for the hydride ligands, and the $^{31}P\{^1H\}$ NMR spectra contain AB spin systems. (See Experimental Section for more details of the NMR spectra.)

The $^{31}P\{^1H\}$ NMR spectra in dichloromethane-d_2 are temperature invariant down to 193 K. However the ^{1}H NMR spectra are temperature dependent. At room temperature, both spectra exhibit, in the high-field region, a single virtual triplet resonance at −11.41 [$J_{HP} + J_{HP'} = 20.8$ (**5**)] and −11.47 [$J_{HP} + J_{HP'} = 25.2$ (**6**)] ppm. This observation is consistent with the operation of two thermally activated site exchange processes for each compound. In both cases, the activation barriers for the two exchange processes are practically the same. Thus, at about 233 K for both compounds, the decoalescence occurs, and leads to the above-mentioned ABCXY spin systems, which become well resolved at 203 K, as shown in Figure 11 for complex **6**. Line shape analysis of the $^1H\{^{31}P\}$ NMR spectra allows the calculation of the rate constants for the H_A-H_C and H_B-H_C thermal exchange processes at different temperatures. The activation parameters obtained from the corresponding Eyring analysis are collected in Table 5.

The T_1 values for the hydrogen nuclei of the OsH_3 units of **5** and **6** were determined over the temperature range 293−213 K. T_1(min) values of 67 (**5**) and 77 ms (**6**) were obtained at 263 K where the spectra show a broad hydride resonance. These values, which are similar to those found for the binuclear complexes $(P^iPr_3)_2H_3Os(\mu\text{-biim})M(COD)$ (M = Rh (81 ms), Ir (76 ms)),[14c] support the hydride character of **5** and **6**, and suggest

Table 6. Coupling Constants as a Function of Temperature for **5** (Rh) and **6** (Ir)

	J_{ac} (Hz)		J_{bc} (Hz)	
T (K)	**5**	**6**	**5**	**6**
203	18.0	16.7	21.3	20.0
193	17.4	14.4	18.9	19.3
183	13.6	11.8	17.4	17.4
178	−	7.9	−	13.2

that the separation between the central hydride ligand (H_C) and those of the corners is about 1.70 Å. The three hydride ligands most probably form a triangle similar to that shown in Figure 2, as has been proved for the binuclear complex $(P^iPr_3)_2H_3Os(\mu\text{-biim})Ir(COD)$ by X-ray diffraction analysis.[14c] In addition, it should be noted that the temperature for which the T_1 of **5** and **6** has a minimum value is higher than that for the binuclear complexes $(P^iPr_3)_2H_3Os(\mu\text{-biim})M(COD)$ (230 K) and for the mononuclear compound $OsH_3(Hbiim)(P^iPr_3)_2$ (210 K). This observation is in agreement with the tetranuclear character of **5** and **6**, which in solution decreases the rate of tumbling of these molecules,[26] compared with the dinuclear and mononuclear derivatives.

At 183 K, the ABC spin systems contained in the $^1H\{^{31}P\}$ NMR spectra are defined by $\delta_A = -11.33$ (**5**) and −11.35 (**6**), $\delta_B = -11.63$ (**5**) and −11.67 (**6**), $\delta_C = -12.69$ (**5**) and −12.71 (**6**), $J_{AC} = 14$ (**5**) and 12 Hz (**6**), $J_{BC} = 17$ (**5**) and 17 Hz (**6**), and $J_{AB} = 0$ Hz (**5** and **6**). Between 178 and 203 K, the values of the chemical shifts of the A, B, and C sites, as well as that of J_{AB}, show no significant temperature dependence. However, the magnitudes of the observed J_{AC} and J_{BC} are sensitive to the temperature, increasing their values as the temperature is increased (Table 6). The temperature-dependent coupling constants between the hydride ligands of **5** and **6** can be readily explained in terms of the exchange coupling phenomenon between the hydridic protons. In this case, the phenomenon seems also to fit into the 2D harmonic oscillator model reported by Heinekey and co-workers.[10d] Assuming the value of a in eq 4 as 1.7 Å, we have estimated that the values of J_{mag} are between 7 and 11 Hz for both compounds.

In addition, it should be pointed out that in **5** and **6** the quantum exchange coupling involves the central hydride and the two hydrides of the corners of the OsH_3 unit, while in **2** there is quantum exchange coupling between the central hydride and one of the two situated in the corners of the OsH_3 unit.

Concluding Remarks

This paper describes the synthesis and characterization of the complexes $OsH_3\{\kappa\text{-}N,\kappa\text{-}S\text{-}(2\text{-Spy})\}(P^iPr_3)_2$ (**2**), $OsH_3\{\kappa\text{-}N,\kappa\text{-}O\text{-}OC(O)CH[CH(CH_3)_2]\ NH_2\}(P^iPr_3)_2$ (**3**), $OsH_3\{\kappa\text{-}N,\kappa\text{-}O\text{-}(2\text{-Opy})\}(P^iPr_3)_2$ (**4**), and $[(P^iPr_3)_2H_3Os(\mu\text{-biim})M(TFB)]_2$ [M = Rh (**5**), Ir (**6**)], containing unsymmetrical OsH_3 units. For compounds **2**−**4**, the asymmetry of the OsH_3 unit is a consequence of the presence in the complexes of a bidentate ligand with two different donor atoms, while for complex **5** and **6** the asymmetry of the OsH_3 units is a result of the asymmetry of the bridging tetradentate metallo-ligands $[M(\mu\text{-biim})M(TFB)]_2^{2-}$ (M = Rh, Ir).

From a structural point of view, the coordination geometry around the osmium atoms of the five complexes can best be described as pentagonal bipyramid, where the hydride ligands are roughly coplanar with the osmium atom and form a triangle with sides of 1.6, 1.8, and between 2.5 and 2.9 Å, respectively. A topological analysis of the electron density of the model complex $OsH_3\{\kappa\text{-}N,\kappa\text{-}S\text{-}(2\text{-Spy})\}(PH_3)_2$ indicates that there is

no bond critical point connecting the hydrogen atoms of the OsH_3 unit, and the map of the Laplacian plot of the computed ρ exhibits three separated charge concentrations associated with each hydride ligand.

In solution the hydride ligands of the five compounds undergo two different thermally activated site exchange processes, which involve the central hydride with each hydride ligand situated cis to the donor atoms of the chelate groups. For all compounds the activation barriers of the two exchange processes are very similar, and theoretical calculations indicate that the transition states of these thermally activated exchange processes have a *cis*-hydride−dihydrogen nature.

Complexes **2**, **5**, and **6** also show quantum exchange coupling, which can be fitted into the 2D harmonic oscillator model recently reported by Heinekey and co-workers.[10d] In complex **2**, the phenomenon involves the central hydride and that situated cis to the sulfur atom of the pyridine-2-thiol group. In **5** and **6** the quantum exchange coupling is observed between the central hydrides and those situated cis to the nitrogen atoms of the tetradentate [M(μ-biim)M(TFB)]$_2$ metallo-ligands.

In conclusion, we report new unsymmetrical MH_3 complexes, which in solution show two different thermally activated site exchange processes between the hydride ligands of the MH_3 unit and, depending upon the nature of the co-ligands, can undergo no, one, or two quantum exchange coupling processes.

Experimental Section

Physical Measurements. ^{1}H, ^{1}H {^{31}P}, and ^{31}P {^{1}H} NMR spectra were recorded on either a Varian XL 200, a Varian UNITY 300, or a Bruker 300 AXR spectrometer. The probe temperature of the NMR spectrometers was calibrated at each temperature against a methanol standard. For the T_1 measurements the 180° pulses were calibrated at each temperature. Chemical shifts are expressed in ppm upfield from Me_4Si (^{1}H) or 85% H_3PO_4 (^{31}P). Coupling constants (J and N [$N = J(PH) + J(P'H)$ or $J(PC) + J(P'C)$]) are given in hertz. The conventional inversion−recovery method (180−τ−90) was used to determine T_1. The Roesy proton experiment was recorded on a Bruker 300 AXR with a mixing time of 100 ms. IR data were recorded on a Nicolet 550 spectrophotometer. Elemental analyses were carried out with a Perkin-Elmer 240C microanalyzer. Mass spectra analyses were performed with a VG Autospec instrument. In FAB$^+$ mode (used for complexes **5** and **6**) ions were produced with the standard Cs^+ gun at ca. 30 kV, and 3-nitrobenzyl alcohol (NBA) was used as the matrix.

Kinetic Analysis. Complete line shape analysis of the spectra ^{1}H-{^{31}P} NMR was achieved using the program DNMR6 (QCPE, Indiana University). The rate constants for various temperatures were obtained by visually matching observed and calculated spectra. The transverse relaxation time, T_2, used was obtained from spectra for all temperatures recorded, from the line width of the aromatic ligand proton resonances. We assume $k_{XYZ} = k_{XY} = 0$ (Z being the central hydride) for all temperatures recorded. For complex **2** the coupling constant used, J_{ac}, was the one observed in the spectra (from 175 to 190 K) or obtained from simulation (from 195 to 210 K). The activation parameters $\Delta H^{\ddagger}$ and $\Delta S^{\ddagger}$ were calculated by a least-squares fit of ln(k/T) vs $1/T$ (Eyring equation). Error analysis assumed a 10% error in the rate constant and 1 K in the temperature. Errors were computed by published methods.[29]

Computational Details. Calculations were performed with the Gaussian 94 series of programs[30] using the density functional theory (DFT)[31] with the B3LYP functional,[32] which has already been used with success to study several dihydrogen and polyhydride systems.[17,23e,33] C_s symmetry was maintained throughout the geometry optimizations. A quasirelativistic effective core potential operator was used to represent the 60 innermost electrons of the osmium atom.[34] The basis set for the metal atom was that associated with the pseudopotential,[34] with a standard double-ζ LANL2DZ contraction.[30] P and S atoms were described with the 6-31G(d) basis set.[35a] The basis set for the hydrogen atoms directly attached to the metal was double-ξ, supplemented with a polarization p shell.[35b,c] The 6-31G basis set was used for the other H atoms, as well as for C and N atoms.[35b] The topological properties of the electron density were calculated with the AIMPAC package.[36]

Synthesis. All reactions were carried out under an argon atmosphere using standard Schlenk techniques. Solvents were dried using appropriate drying agents and freshly distilled under argon before use. The starting complexes $OsH_6(PiPr_3)_2$,[37] $OsH_3(Hbiim)(P^iPr_3)_2$,[14c] and [M(μ-OMe)(TFB)]$_2$ (M = Rh,[38] Ir[39]) were prepared by published methods.

Preparation of $OsH_3\{\kappa$-*N*,κ-*S*-(2-Spy)$\}(P^iPr_3)_2$ (2). A colorless solution of $OsH_6(P^iPr_3)_2$ (**1**) (180 mg, 0.35 mmol) in 16 mL of toluene was treated with pyridine-2-thiol (39 mg, 0.35 mmol) and heated under reflux for 2 h. The yellow solution was filtered through Kieselguhr and concentrated to ca. 0.5 mL. Addition of methanol caused the precipitation of a yellow solid. The solvent was decanted, and the solid was washed twice with methanol and dried in vacuo: yield, 194 mg (89%). Anal. Calcd for $C_{23}H_{49}NOsP_2S$: C, 44.27; H, 7.93; N, 2.24. Found: C, 44.60; H, 8.63; N, 2.02. IR (Nujol): ν(OsH) 2120 cm^{-1}. ^{1}H NMR (300 MHz, C_6D_6, 293 K): δ 8.12 (d, J(HH) = 5.6 Hz, 1H, 2-Spy) 6.60 (t, J(HH) = 7.7 Hz, 1H, 2-Spy), 6.51 (d, J(HH) = 8.3 Hz, 1H, 2-Spy), 6.20 (t, J(HH) = 6.4 Hz, 1H, 2-Spy), 2.2 (m, 6 H, PC*H*CH$_3$), 1.23 (dvt, N = 12.9 Hz, J(HH) = 6.9 Hz, 18 H, PCHC*H*$_3$), 1.06 (dvt, N = 12.5 Hz, J(HH) = 6.4 Hz, 18 H, PCHC*H*$_3$), −11.53 (t, J(PH) = 12.8 Hz, 3H, OsH). ^{31}P{^{1}H} NMR (121.42 MHz, C_6D_6, 293 K): δ 24.0 (s).

Preparation of $OsH_3\{\kappa$-*N*,κ-*O*-OC(O)CH[CH(CH$_3$)$_2$]NH$_2\}(P^iPr_3)_2$ (3). This complex was prepared analogously to that described for **2**, starting from $OsH_6(P^iPr_3)_2$ (**1**) (180 mg, 0.35 mmol) and L-valine (41 mg, 0.35 mmol). In this case, the mixture was heated under reflux for 1 h. A white solid was formed after addition of hexane. Yield: 198 mg (90%). Anal. Calcd for $C_{23}H_{55}NO_2OsP_2$: C, 43.85; H, 8.8; N, 2.22. Found: C, 43.82; H, 9.53; N, 2.16. IR (Nujol): ν(NH$_2$) 3135, 3060, ν(OsH) 2130, ν(OCO) 1650 cm^{-1}. ^{1}H NMR (300 MHz, C_6D_6, 293 K): δ 3.71, 3.25 (br, each 1 H, NH$_2$), 3.01 (ddd, J(HH) = 3.0, 6.3, and 12.4 Hz, 1 H, CH), 2.74 (m, 1 H, CH), 1.86 (m, 6 H, PC*H*CH$_3$), 1.11 (m, 36 H, PCHC*H*$_3$), 0.90 (d, J(HH) = 6.9 Hz, 3 H, CH$_3$), 0.77 (d,

(29) Morse, P. M.; Spencer, M. O.; Wilson, S. R.; Girolami, G. S. *Organometallics* **1994**, *13*, 1646.
(30) Frisch, M. J.; Trucks, G. W.; Schlegel, H. B.; Gill, P. M. W.; Johnson, B. G.; Robb, M. A.; Cheeseman, J. R.; Keith, T. A.; Petersson, G. A.; Montgomery, J. A.; Raghavachari, K.; Al-Laham, M. A.; Zakrzewski, V. G.; Ortiz, J. V.; Foresman, J. B.; Cioslowsky, J.; Stefanov, B. B.; Nanayakkara, A.; Challacombe, M.; Peng, C. Y.; Ayala, P. Y.; Chen, W.; Wong, M. W.; Andrés, J. L.; Replogle, E. S.; Gomperts, R.; Martin, R. L.; Fox, D. J.; Binkley, J. S.; Defrees, D. J.; Baker, J.; Stewart, J. J P.; Head-Gordon, M.; Gonzalez, C.; Pople, J. A. *Gaussian 94*; Gaussian Inc.: Pittsburgh, PA, 1995.
(31) (a) Parr, R. G.; Yang, W. *Density Functional Theory of Atoms and Molecules*; Oxford University Press: Oxford, U.K., 1989. (b) Ziegler, T. *Chem. Rev.* **1991**, *91*, 651.
(32) (a) Lee, C.; Yang, W.; Parr, R. G. *Phys. Rev. B* **1988**, *37*, 785. (b) Becke, A. D. *J. Chem. Phys.* **1993**, *98*, 5648. (c) Stephens, P. J.; Devlin, F. J.; Chabalowski, C. F.; Frisch, M. J. *J. Phys. Chem.* **1994**, *98*, 11623.
(33) (a) Bacskay, G. B.; Bytheway, I.; Hush, N. S. *J. Am. Chem. Soc.* **1996**, *118*, 3753. (b) Bytheway, I.; Backsay, G. B.; Hush, N. S. *J. Phys. Chem.* **1996**, *100*, 6023. (c) Gelabert, R.; Moreno, M.; Lluch, J. M.; Lledós, A. *J. Am. Chem. Soc.* **1997**, *119*, 9840.
(34) Hay, P. J.; Wadt, W. R. *J. Chem. Phys.* **1985**, *82*, 299.
(35) (a) Francl, M. M.; Pietro, W. J.; Hehre, W. J.; Binkley, J. S.; Gordon, M. S.; Defrees, D. J.; Pople, J. A. *J. Chem. Phys.* **1982**, *77*, 3654. (b) Hehre, W. J.; Ditchfield, R.; Pople, J. A. *J. Chem. Phys.* **1972**, *56*, 2257. (c) Hariharan, P. C.; Pople, J. A. *Theor. Chim. Acta* **1973**, *28*, 213.
(36) Biegler-Köning, F. W.; Bader, R. F. W.; Tang, T. H. *J. Comput. Chem.* **1982**, *3*, 317.
(37) Aracama, M.; Esteruelas, M. A.; Lahoz, F. J.; López, J. A.; Meyer, U.; Oro, L. A.; Werner, H. *Inorg. Chem.* **1991**, *30*, 288.
(38) Usón, R.; Oro, L. A.; Cabeza, J. A. *Inorg. Synth.* **1985**, *23*, 126.
(39) Usón, R.; Oro, L. A.; Carmona, D.; Esteruelas, M. A.; Foces-Foces, C.; Cano, F. H.; García-Blanco, S.; Vázquez de Miguel, A. *J. Organomet. Chem.* **1984**, *273*, 111.

J(HH) = 7.1 Hz, 3 H, CH_3), −13.90 (br, 3H, OsH). $^{31}P\{^1H\}$ NMR (80.98 MHz, CD_2Cl_2, 293 K): δ 32.5, 30.0 (AB system, J(PP′) = 285 Hz).

Preparation of $OsH_3\{\kappa$-*N*,κ-*O*-(2-Opy)$\}(P^iPr_3)_2$ (4). This complex was prepared analogously to that described for **2**, starting from $OsH_6(P^iPr_3)_2$ (**1**) (180 mg, 0.35 mmol) and 2-hydroxypyridine (33 mg, 0.35 mmol). In this case, the mixture was heated under reflux for 20 min. A yellow solid was formed after storing at −78 °C in hexane for 3 h. Yield: 138 mg (65%). Anal. Calcd for $C_{23}H_{49}NOOsP_2$: C, 45.44; H, 8.14; N, 2.30. Found: C, 45.91; H, 8.42; N, 2.57. IR (Nujol): ν(OsH) 2208, 2140, 2120 cm^{-1}. ^1H NMR (300 MHz, C_6D_6, 293 K): δ 7.90 (d, J(HH) = 4.7 Hz, 1H, 2-Opy), 6.91 (t, J(HH) = 7.8 Hz, 1H, 2-Opy), 6.23 (t, J(HH) = 5.8 Hz, 1H, 2-Opy), 6.01 (d, J(HH) = 8.6 Hz, 1H, 2-Opy), 1.92 (m, 6 H, PC*H*CH_3), 1.16 (dvt, N = 12.6 Hz, J(HH)= 6.9 Hz, 18 H, PCHC*H*$_3$), 1.13 (dvt, N = 12.7 Hz, J(HH) = 7.0 Hz, 18 H, PCHC*H*$_3$), −12.7 (br, 3H, OsH). $^{31}P\{^1H\}$ NMR (121.42 MHz, C_6D_6, 293 K): δ 33.2 (s).

Preparation of $[(P^iPr_3)_2H_3Os(\mu$-biim)Rh(TFB)$]_2$ (5). A suspension of OsH_3(Hbiim)$(P^iPr_3)_2$ (150 mg, 0.23 mmol) in 20 mL of acetone was treated with $[Rh(\mu$-OMe)(TFB)$]_2$ (84 mg, 0.12 mmol). The resulting mixture was stirred while heating under reflux for 7 h after which time an orange solid had formed. The mixture was then cooled to 0 °C, and the solvent was decanted. The solid was washed twice with methanol and dried in vacuo. Yield 150 mg (67%). Anal. Calcd for $C_{72}H_{110}F_8N_8Os_2P_4Rh_2$: C, 44.35; H, 5.69; N, 5.75. Found: C, 44.74; H, 6.12; N, 5.39. IR (Nujol): ν(OsH) 2090, 2070 cm^{-1}. ^1H NMR (300 MHz, C_6D_6, 293 K): δ 7.38, 7.01 (both br, each 4 H, =CH biim), 6.33, 5.45 (both unresolved t, each 2 H, −CH TFB), 3.81 (br, 8 H, =CH TFB),[40] 1.68 (br, 6 H, PC*H*CH_3), 1.53 (br, 6 H, PC*H*CH_3), 0.96 (br, 56 H, PCHC*H*$_3$), 0.69 (br, 16 H, PCHC*H*$_3$), −11.41 (vt, N = 20.8 Hz, 6 H, OsH). $^{31}P\{^1H\}$ NMR (121.42 MHz, C_6D_6, 293 K): δ 20.9 and 20.8 (central signals of an AB spin system). MS (FAB^+): *m*/*e* 1951 (M^+).

Preparation of $[(P^iPr_3)_2H_3Os(\mu$-biim)Ir(TFB)$]_2$ (6). This complex was prepared analogously to **5**, starting from OsH_3(Hbiim)$(P^iPr_3)_2$ (150 mg, 0.23 mmol) and $[Ir(\mu$-OMe)(TFB)$]_2$ (109 mg, 0.12 mmol). A garnet solid was formed. Yield: 147 mg (60%). Anal. Calcd for $C_{72}F_8H_{110}Ir_2N_8Os_2P_4$: C, 40.63; H, 5.21; N, 5.26. Found: C, 40.39; H, 5.43; N, 5.07. IR (Nujol): ν(OsH) 2115, 2095 cm^{-1}. ^1H NMR (300 MHz, C_6D_6, 293 K): δ 7.38, 7.22, 6.94, 6.85 (each br, each 2 H, =CH biim), 6.40, 5.52 (both unresolved t, each 2 H −CH TFB), 3.20, 3.03, 2.86, 2.43 (each br, each 2 H, =CH TFB), 1.70 (br, 6 H, PC*H*CH_3), 1.51 (br, 6 H, PC*H*CH_3), 1.01 (br, 56 H, PCHC*H*$_3$), 0.67 (br, 16 H, PCHC*H*$_3$), −11.47 (vt, N = 25.2 Hz, 6 H, OsH). $^{31}P\{^1H\}$ NMR (121.42 MHz, C_6D_6, 293 K): δ 22.0 and 21.9 (central signals of an AB spin system). MS (FAB^+): *m*/*e* 2131 (M^+).

(40) In CD_2Cl_2 at 263 K.; δ: 4.33, 4.00, 3.65, and 2.67 (each br, each 2 H, =CH TFB).

Table 7. Crystal Data and X-ray Data Collection and Refinement for $OsH_3\{\kappa$-*N*,κ-*S*-(2-Spy)$\}(P^iPr_3)_2$ (**2**)

formula	$C_{23}H_{49}NOsP_2S$	space group	*P*21/*c*
fw	623.85	*V*, Å^3	2756(1)
a, Å	8.832(2)	*Z*	4
b, Å	21.124(5)	ρ (g cm^{-3})	1.504
c, Å	14.923(4)	*T* (K)	230
β, (deg)	98.23(3)	λ (Mo Kα), Å	0.710 73
R,[a] R_w[b] (obs. data)	0.0301, 0.328	μ, mm^{-1}	4.8

[a] $R = \sum|[F(\text{obs}) - F(\text{calc})]|/\sum F(\text{obs})$. [b] $R_w = \sum w^{1/2}|[F(\text{obs}) - F(\text{calc})]|/\sum w^{1/2}F(\text{obs})$.

X-ray Structure Analysis of Complex $OsH_3\{\kappa$-*N*,κ-*S*-(2-Spy)$\}(P^iPr_3)_2$ (2). Crystals suitable for an X-ray diffraction study were obtained by slow diffusion of methanol into a saturated solution of **2** in toluene. A summary of crystal data and refinement parameters is reported in Table 7. A yellow crystal, of approximate dimensions 0.7 × 0.67 × 0.33 mm, was glued on a glass fibber and mounted on a Siemens-STOE AED-2 diffractometer. A group of 64 reflections in the range $20 \le 2\theta \le 40°$ were carefully centered at 230 K and used to obtain, by least-squares methods, the unit cell dimensions. Three standard reflections were monitored at periodic intervals throughout data collection: no significant variations were observed. All data were corrected for absorption using a semiempirical method.[41] The structure was solved by Patterson (Os atom) and conventional Fourier techniques and refined by full-matrix least-squares (SHELXTL-PLUS[42]). Anisotropic parameters were used in the last cycles of refinement for all non-hydrogen atoms. The three hydride ligands were refined as free isotropic atoms. The remaining hydrogen atoms were located from difference Fourier maps or fixed in idealized positions and refined riding on carbon atoms with a common isotropic thermal parameter. The refinement converge to $R = 0.0301$ and $R_w = 0.0328$ [observed data], with weighting scheme $w^{-1} = \sigma^2(F) + 0.000725(F^2)$.

Acknowledgment. We thank the DGICYT of Spain (Projects PB95-0806 and PB95-0639-CO2-01, Programa de Promoción General del Conocimiento). The use of computational facilities of the Centre de Supercomputació i Comunicacions de Catàlunya (C^4) is gratefully appreciated.

Supporting Information Available: An X-ray crystallographic file, in CIF format, for complex **2** is available free of charge via the Internet at http://pubs.acs.org.

IC9804061

(41) North, A. C. T.; Phillips, D. C.; Mathews, F. S. *Acta Crystallogr.* **1968**, *A24*, 351.
(42) Sheldrick, G. *SHELXTL-PLUS*; Siemens Analytical X-ray Instruments, Inc.: Madison, WI, 1990.